Project for the course
Functional Materials TFY4220 at NTNU Trondheim

Photonic Crystals

Matthias Schrade Heike Pfau

26.10.2007

Contents

1 Introduction

Photonic crystals (PhCs) are a new class of materials that have the ability to manipulate and control the propagation of light. Properly designed, PhCs can either prohibit the propagation of electromagnetic waves, allow it only in certain frequency ranges or localize light in specific areas. The concept of PhCs and the photonic band structure can be seen as an analogy to the electric conduction process and the electron band structure. The term Photonic Crystal is used for every periodically structured dielectric or metallic material, whereas only particular materials show a photonic band gap (PBG) and are referred to as Photonic Band Gap Materials.

The simplest form of a PhC, a 1D periodic structure, was already studied regarding its interesting optical properties more than 100 years ago by Lord Rayleigh. Forty years after E. Purcell sketched the possibility of prohibited spontaneous emission in some materials [1], E. Yablonovitch came up with the idea of 2D- and 3D photonic crystals, expecting a PBG [2]. In the last 20 years, such structures have seen an increasing interest added by the simultaneous improvement of fabrication precision. They show many interesting properties, like inhibited spontaneous emission, low-loss waveguiding, a significant reduction of the group velocity and their particular properties can be changed and controlled in the fabrication process.

Nowadays PhCs are used in a broad range of applications like LEDs, lasers and optical fibres. There are even some examples of natural occurring PhCs, e.g. the opal which optical appearence is due to Braggreflexion in its microstructure. Other examples are the wings of some butterflies or the hair of the sea mouse.

We will start with the physical background of photonic crystals and certain calculation methods. The third chapter presents the fabrication of PhCs, considering different materials and 3D-fabrication. Finally we specify several applications, illustrated by some particular research projects.

2 Theoretical Overview

The theory of electromagnetic waves in photonic crystals is similar in many aspects with the theory of electron waves in an atomic lattice. Hence a lot of concepts for describing electromagnetic waves are borrowed from solid state physics. The analogy of both phenomena starts in the formal relation between MAXWELL's equations for electromagnetic waves in a dielectric medium and the SCHRÖDINGER equation for massive particles in a potential. A comparison will show that the dielectric permittivity for the photons is the same as the potential for the electrons. And in the end it leads to the BLOCH-FLOQUET theorem for periodical structures i.e. for electrons to the COULOMB potential and for photons to the periodicy of the dielectric permittivity in form of a lattice out of different materials. The result in both cases will be dispersion relations and band structures with band gaps. But the theory in solid state physics is not completely applicable to photonic crystals. Differences are based e.g. in the vectorial character of the electromagnetic field in contrast to the scalar field of electron waves or in the spin character of photons, which are bosons, and electrons, which are fermions.

In this chapter we want to give an introduction into the main aspects of the theory of photonic crystals. We will describe the calculation of the band structure of a photonic crystal and the occurence of the photonic band gap for one and more dimensions. To simplify the calculations we will use the "plane wave method" which, however, leeds to some problems in numerical calculations but it is still an important model to describe photonic crystals.

2.1 Wave Equation and Eigenvalue Problem

The electromagnetic field is discribed by MAXWELL's equations. We assume that there are no free charges and no electric currents in our medium. In this case, MAXWELL's equations have the following form.

$$\begin{aligned} \boldsymbol{\nabla} \cdot \boldsymbol{D}(\boldsymbol{r},t) &= 0 \\ \boldsymbol{\nabla} \cdot \boldsymbol{B}(\boldsymbol{r},t) &= 0 \\ \boldsymbol{\nabla} \times \boldsymbol{E}(\boldsymbol{r},t) &= -\frac{\partial}{\partial t}\boldsymbol{B}(\boldsymbol{r},t) \\ \boldsymbol{\nabla} \times \boldsymbol{H}(\boldsymbol{r},t) &= -\frac{\partial}{\partial t}\boldsymbol{D}(\boldsymbol{r},t) \end{aligned} \tag{1}$$

Here $\boldsymbol{E}$ represents the electric field, $\boldsymbol{H}$ the magnetic field, $\boldsymbol{D}$ the electric displacement and $\boldsymbol{B}$ the magnetic induction. To solve this equations we replace the magnetic induction $\boldsymbol{B}$ by the magnetic field $\boldsymbol{H}$ and likewise $\boldsymbol{E}$ by $\boldsymbol{D}$.

$$\boldsymbol{B}(\boldsymbol{r},t) = \mu_0\mu(\boldsymbol{r})\boldsymbol{H}(\boldsymbol{r},t) \tag{2}$$

$$\boldsymbol{D}(\boldsymbol{r},t) = \epsilon_0\epsilon(\boldsymbol{r})\boldsymbol{E}(\boldsymbol{r},t) \tag{3}$$

Generally the magnetic permeability $\mu(\boldsymbol{r})$ and the dielectric constant $\epsilon(\boldsymbol{r})$ are tensors. In our homogenic case they can be treated as scalars. Furthermore we assumed that the

magnetic permeability of the photonic crystal is the same as in free space, $\mu(\boldsymbol{r}) = 1$, and that the dielectric constant $\epsilon(\boldsymbol{r})$ is not dependent on frequency. By inserting these equations (2) and (3) in (1) we obtain the wave equations for $\boldsymbol{E}$ and $\boldsymbol{H}$,

$$\begin{aligned} \frac{1}{\epsilon(\boldsymbol{r})}\boldsymbol{\nabla}\times\{\boldsymbol{\nabla}\times\boldsymbol{E}(\boldsymbol{r},t)\} &= -\frac{1}{c^2}\frac{\partial^2}{\partial t^2}\boldsymbol{E}(\boldsymbol{r},t) \\ \boldsymbol{\nabla}\times\left\{\frac{1}{\epsilon(\boldsymbol{r})}\boldsymbol{\nabla}\times\boldsymbol{H}(\boldsymbol{r},t)\right\} &= -\frac{1}{c^2}\frac{\partial^2}{\partial t^2}\boldsymbol{H}(\boldsymbol{r},t)\,, \end{aligned} \tag{4}$$

where $c = (\mu_0\epsilon_0)^{-1/2}$ is the velocity of light.

Originating in a harmonic time dependence for $\boldsymbol{E}$ and $\boldsymbol{H}$,

$$\begin{aligned} \boldsymbol{E}(\boldsymbol{r},t) &= \boldsymbol{E}(\boldsymbol{r})e^{-i\omega t} \\ \boldsymbol{H}(\boldsymbol{r},t) &= \boldsymbol{H}(\boldsymbol{r})e^{-i\omega t} \end{aligned} \tag{5}$$

the eigenfunctions $\boldsymbol{E}(\boldsymbol{r})$ and $\boldsymbol{H}(\boldsymbol{r})$ will satisfy the time independent wave equations

$$\begin{aligned} \frac{1}{\epsilon(\boldsymbol{r})}\boldsymbol{\nabla}\times\{\boldsymbol{\nabla}\times\boldsymbol{E}(\boldsymbol{r})\} &= -\frac{\omega^2}{c^2}\boldsymbol{E}(\boldsymbol{r}) \\ \boldsymbol{\nabla}\times\left\{\frac{1}{\epsilon(\boldsymbol{r})}\boldsymbol{\nabla}\times\boldsymbol{H}(\boldsymbol{r})\right\} &= -\frac{\omega^2}{c^2}\boldsymbol{h}(\boldsymbol{r})\,. \end{aligned} \tag{6}$$

These equations have a high similarity to the Schrödinger equation for electronic waves in a potential [3],

$$\boldsymbol{\nabla}^2\Psi(\boldsymbol{r}) = -\frac{2m}{\hbar^2}\left\{E - V(\boldsymbol{r})\right\}\Psi(\boldsymbol{r})\,, \tag{7}$$

where $\Psi(\boldsymbol{r})$ is the scalar wave function for an electron with the mass m and $V(\boldsymbol{r})$ is the the potential. Comparing equation (6) with (7) one can recognize the mentioned analogy between the dielectric permittivity $\epsilon(\boldsymbol{r})$ and the potential $V(\boldsymbol{r})$.

Like $V(\boldsymbol{r})$ in a lattice $\epsilon(\boldsymbol{r})$ is a periodic function of $\boldsymbol{r}$ with

$$\epsilon(\boldsymbol{r} + \boldsymbol{a_i}) = \epsilon(\boldsymbol{r}) \qquad (i = 1, 2, 3)\,, \tag{8}$$

where $\{\boldsymbol{a_i}\}$ are the elementary lattice vectors of the photonic crystal.

Therefore we transfer Bloch-Floquet's theorem from solid state physics to photonic crystals and express the fields $\boldsymbol{E}(\boldsymbol{r})$ and $\boldsymbol{H}(\boldsymbol{r})$ with $\{\boldsymbol{a_i}\}$-periodic functions $\boldsymbol{u_{kn}}$ and $\boldsymbol{v_{kn}}$ as [4]

$$\begin{aligned} \boldsymbol{E}(\boldsymbol{r}) &= \boldsymbol{E_{kn}}(\boldsymbol{r}) = \boldsymbol{u_{kn}}(\boldsymbol{r})e^{i\boldsymbol{kr}} \\ \boldsymbol{H}(\boldsymbol{r}) &= \boldsymbol{H_{kn}}(\boldsymbol{r}) = \boldsymbol{v_{kn}}(\boldsymbol{r})e^{i\boldsymbol{kr}} \end{aligned} \tag{9}$$

Because of the periodicity of $\boldsymbol{u_{kn}}$, $\boldsymbol{v_{kn}}$ and $\epsilon(\boldsymbol{r})$, they can be expended in Fourier series, whereas in our case we will expend $\epsilon^{-1}(\boldsymbol{r})$. This results in the following expres-

sions.

$$\begin{aligned} \frac{1}{\epsilon(\boldsymbol{r})} &= \sum_{\boldsymbol{G}} \kappa_{\boldsymbol{G}} e^{i\boldsymbol{G}\boldsymbol{r}} \\ \boldsymbol{E}_{\boldsymbol{k}n}(\boldsymbol{r}) &= \sum_{\boldsymbol{G}} \boldsymbol{E}_{\boldsymbol{k}n}(\boldsymbol{G}) e^{i(\boldsymbol{k}+\boldsymbol{G})\boldsymbol{r}} \\ \boldsymbol{H}_{\boldsymbol{k}n}(\boldsymbol{r}) &= \sum_{\boldsymbol{G}} \boldsymbol{H}_{\boldsymbol{k}n}(\boldsymbol{G}) e^{i(\boldsymbol{k}+\boldsymbol{G})\boldsymbol{r}} \,, \end{aligned} \tag{10}$$

where $\kappa(\boldsymbol{G})$, $\boldsymbol{E}_{\boldsymbol{k}n}(\boldsymbol{G})$ and $\boldsymbol{H}_{\boldsymbol{k}n}(\boldsymbol{G})$ are the FOURIER coefficients in reciprocal space. Now inserting the expansions (10) into the wave equations (6) the eigenvalue equations get the following form [4].

$$\begin{aligned} -\sum_{\boldsymbol{G'}} \kappa_{\boldsymbol{G}-\boldsymbol{G'}} \left(\boldsymbol{k}+\boldsymbol{G'}\right) \times \left\{ \left(\boldsymbol{k}+\boldsymbol{G'}\right) \times \boldsymbol{E}_{\boldsymbol{k}n}(\boldsymbol{G'}) \right\} &= \frac{\omega_{\boldsymbol{k}n}^2}{c^2} \boldsymbol{E}_{\boldsymbol{k}n}(\boldsymbol{G}) \\ -\sum_{\boldsymbol{G'}} \kappa_{\boldsymbol{G}-\boldsymbol{G'}} \left(\boldsymbol{k}+\boldsymbol{G}\right) \times \left\{ \left(\boldsymbol{k}+\boldsymbol{G'}\right) \times \boldsymbol{H}_{\boldsymbol{k}n}(\boldsymbol{G'}) \right\} &= \frac{\omega_{\boldsymbol{k}n}^2}{c^2} \boldsymbol{H}_{\boldsymbol{k}n}(\boldsymbol{G}) \,, \end{aligned} \tag{11}$$

where $\omega_{\boldsymbol{k}n}^2$ denotes the eigenfrequency of the eigenvectors $\boldsymbol{E}_{\boldsymbol{k}n}(\boldsymbol{G})$ and $\boldsymbol{H}_{\boldsymbol{k}n}(\boldsymbol{G})$. Normally these sets of equations (11) can only be solved numerically and it leads to the dispersion relations and the band structure of photonic crystals. That points to the field of research for new methods of modelling systems of photonic crytsals. There are several other methods despite the "plane wave method" to get an expression for the dispersion relation or band structure which often deliver more exactly results but change nothing in the general properties.

2.2 The Photonic Band Diagram

As for electrons in an atomic lattice the calculation of the dispersion relation for photonic crystals in form of $\omega(\boldsymbol{k})$ leads to the occurence of allowed and forbidden bands which can be plotted in a band diagram. In what follows, we want to describe the occurence of photonic bands in one-, two- and tree dimensional photonic crystals which are schematically shown in Fig. 1.

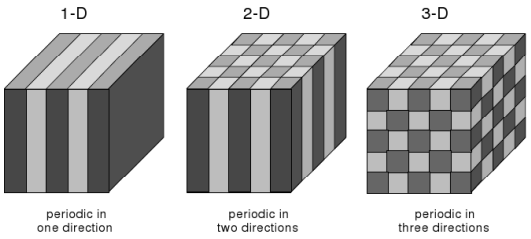

Fig. 1: Schematic structure of one, two and tree dimensional photonic crystals where the periodicy is constructed out of differences in the dielectric permittivity [5]

2.2.1 One-Dimensional Photonic Crystals

To illustrate the results of the last chapter, we will have a closer look to one dimensional (1D) photonic crystals. We will discuss a system shown in the left side of Fig. 1 which consists of layers out of two materials A_1 and A_2 with the dielectric constants ϵ_1 and ϵ_2. Assume a periodic condition for the layers like

$$\epsilon(x+a) = \epsilon(x)\,. \tag{12}$$

In this 1D case the wave equations for the electric field $\boldsymbol{E}$ reduce to

$$\frac{1}{\epsilon(x)}\frac{\partial^2}{\partial x^2}\boldsymbol{E}(x,t) = \frac{1}{c^2}\frac{\partial^2}{\partial t^2}\boldsymbol{E}(x,t) \tag{13}$$

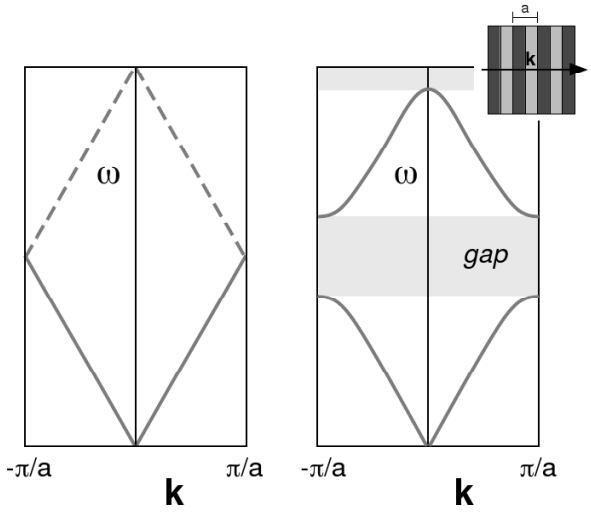

Fig. 2: *Left.* Schematic 1D band diagram (dispersion relation) for a uniform medium where the dashed lines showing the "folded" dispersion relation. *Right.* Schematic 1D band diagram for periodic dielectric medium with occuring bad gaps [5]

Consider now a system with an uniform $\epsilon = 1$. This leads to a plane wave solution for the electric field in equation (13) and the dispersion relation

$$\omega(k) = ck\,, \tag{14}$$

which is shown on the left side of Fig. 2. Because of the periodicy it is possible to describe the states in form of Bloch functions like in the equations (9) and to reduce the representation of the dispersion relation to the first Brillouin zone, here from $k = -\pi/a$ to $k = +\pi/a$, by "folding" the dispersion relation. Now, the $k = -\pi/a$ mode has an equivalent wave vector like the $k = \pi/a$ mode and they have the same frequency. Here at the border of the Brillouin zone the Bragg condition $\Delta\boldsymbol{k} = \boldsymbol{G}$ is valid and leads to

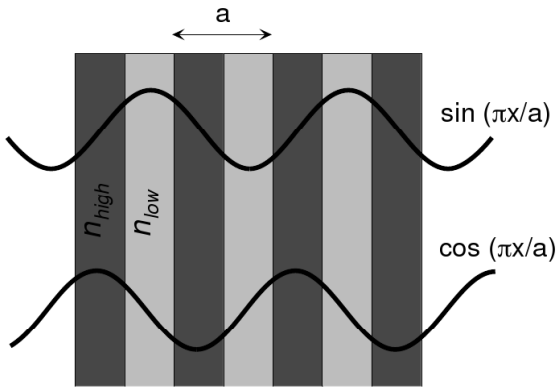

Fig. 3: Schematic origin of the 1D band gap. The degenerated wave functions at $k = \pm\pi/a$ split into two standing waves forming the lower and the upper edge of the gap [5]

a coherent back scattering. Therefore, instead of writing this wave solution with the electric field $E \sim e^{\pm i\pi x/a}$ we can split it into two standing waves [5],

$$E_- \sim \sin \pi x/a \tag{15}$$

$$E_+ \sim \cos \pi x/a\,, \tag{16}$$

which are shown in Fig. 3. Suppose now that the dielectric constant is sinusoidal perturbated with a period a.

$$\epsilon(x) = 1 + \Delta \cos 2\pi x/a \tag{17}$$

In the presence of this oscillating dielectric constant the degenaracy of the two fields E_- and E_+ is broken and we get two different frequencies for the two wave functions. Assuming $\Delta > 0$ then the field E_- is more concentrated in lower-ϵ region while E_+ is more concentrated in higher-ϵ regions as shown in Fig. 3. In analogy to elcetronic waves [6] the energy of the "air" band E_- is higher than the energy of the "dielectric" band E_+. Consequently the frequency is lower for E_- and higher for E_+. The result is a band gap, which is shown on the right side of Fig. 2, where a propagation of electromagnetic waves is prohibited. From pertubation therory one can show that for $\Delta \ll 1$ the band gap is $\Delta\omega/\omega \cong \Delta/2$ [5].

2.2.2 Two-Dimensional Photonic Crystals

The analysis of one-dimensional structures in the former chapter revealed fundamental properties of photonic crysals, but it was in principle nothing more than a transfer of the theory for electronic waves in a atomic lattice to electromagnetic waves and offers less new aspects. This will change for higher dimensional systems where not only the propagation direction of the waves has to be considered but also the polarisation of the wave has a significant influence for the band diagrams. For this reason it is hard to recieve a omnidirectional and complete band gap for higher dimensional photonic

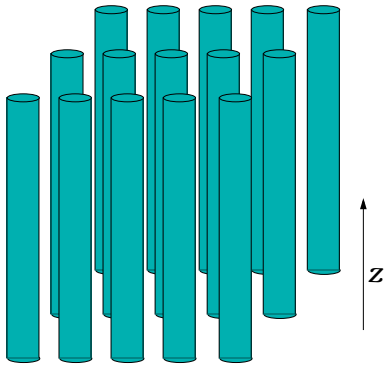

Fig. 4: 2D crystal out of cylindrical rods

crystals. In what follows, we want to discribe band diagrams of 2D crystals and figure out which influence the polarization has on the origin of band gaps.

Imagine a two 2D lattice built out of rods as shown in Fig. 4. So we have two possible polarisations: transverse electric (TE), where the magnetic field is along the z-direction of the rods and the electric field perpendicular to it in the x-y plane, and transversal magnetic (TM), where the electric field is along the rods and the magnetic perpendicular.

We will look at a hexagonal structure of rods which is shown in Fig. 5 together with the (irriducible) Brillouin zone. Now we fill the rods with a dielectric material with $\epsilon > 1$ and the surounding material is supposed to be air (Fig. 5 *top*). The calculated band diagram shows the bands for TE (solid) and TM (dashed) polarisation. The same is done for air rods in a dielectric medium in the lower part of the figure. The most important result is the different behaviour of the two different polarized waves which leads to different band gaps for these polarisations: In the first example occurs a band gap only for the TM polarisation while in the second diagram a TE band gap is revealed. Therefore in both cases it exists no complete band gap which would only occure when both TE and TM polarisation provide a band gap in the same frequency region.

The reason for this different behaviour of TM and TE polarized light can be explained by the boundary conditions of the electric and magnetic field for crossing dielectrical interfaces. We will have a closer look to the first example with dielectric rods in air. The electric field for TM modes, which is parallel to the rods, remains when crossing the interface. Therefore the displacement $\boldsymbol{D} = \epsilon \boldsymbol{E}$ is strongly localised within the cylinders and minimizes the energy of the fundamental mode for the same reason as discribed for the 1D crystal. For the first excited mode the filed is mostly localized in the air region and therefore enhance the energy. This leeds to an enlarged separation of the two modes. For the TE modes, where the electric field is perpendicular to the rods, the field lines have to cross the air regions to enter the next rod. This enhance the energy in both the fundamental and the excited mode. The result is a much smaller separation and a generally higher energy of the TE modes. An analog explanation can be given for the air rods in a dielectric substrat in the lower part of Fig. 5.

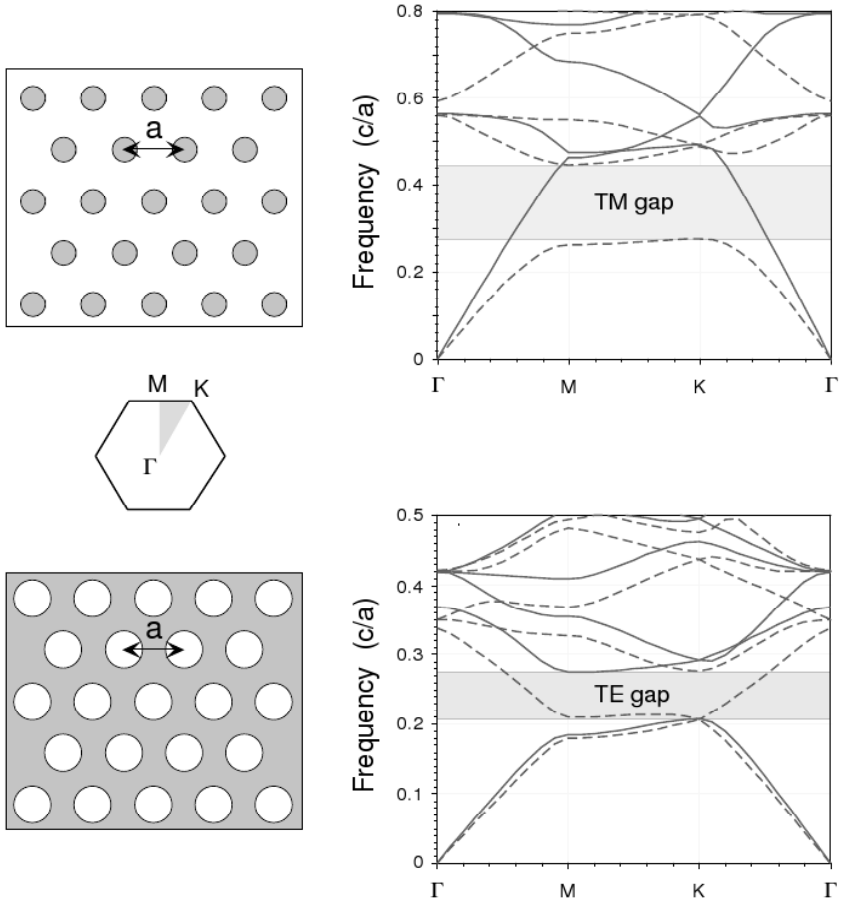

Fig. 5: 2D hexagonal lattice with dielectric rods ($\epsilon = 12$, $r = 0.2a$) in air (*top*) and air rods ($r = 0.3a$) in a dielectric substrat (*bottom*) together with the Brillouin zone and the calculated band diagrams around the irreducible Brillouin zone (shaded triangle) where TE/TM polarisation are denoted by solid/dashed lines [5]

2.2.3 Tree-Dimensional Photonic Crystals

A complete photonic bandgap for all polarisations and propagation directions of the waves can only be realised for tree dimensional (3D) photonic crystals. The first 3D crystal with a full photonic band gap was fabricated by Yablonovitch et al. [7] in 1991 and consists of a fcc structure. This structure in real space leads to the "roundest" structure in reciprocal space which provides the highest prospects for a complete photonic band gap. The "atoms" have a shape of spherical voids in a dielectric background. This structure is now called Yablonovite. Fig. 6.

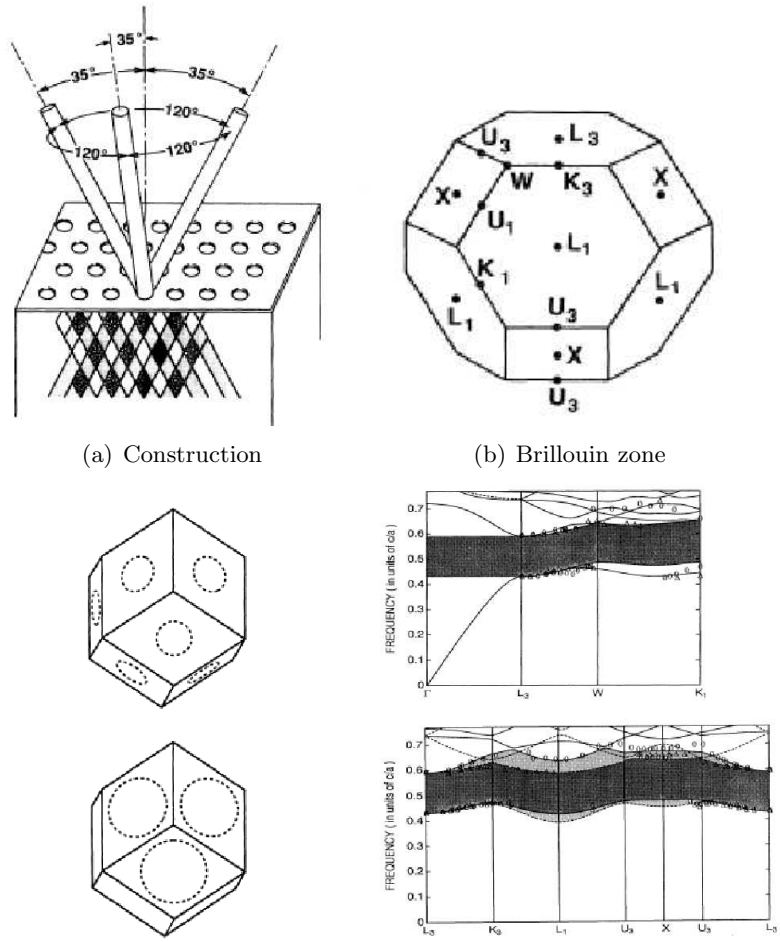

(a) Construction (b) Brillouin zone

(c) Wiegner-Seitz real space unit cell (d) Band diagram with band gap

Fig. 6: The Yablonovite with its fcc structure as the first produced photonic crystal with a omnidirectional band gap [7].

2.3 Defects

There exist two main types of defects: point defects, which are very local disruptions and cause electromagnetic modes at discrete frequencies like the isolated electric states, and extended defects which are analog to dislocations of a crystal and result in transmission bands in the region of the PBG. Thus, defects in PhCs can be compered with the doping of a semiconductor.

The existence of defects may lead to singularities in the density of states (Chap. 2.4) e.g. for single point defect it occures a Delta function in a complete PBG as can be seen in Fig. 10.

2.3.1 Point Defects

For a 1D photonic crystals point defects can be obtained by two different manipulations: changing of the size of one "atom" in the crystal or modifying the refractive index of this one. Thus, such point defects is nothing more than a FABRY-PEROT cavity [3] which is shown in Fig. 7. Electromagnetic modes will be therefore occure at discrete frequencies.

Fig. 7: Point defect in a 1D crystal (FABRY-PEROT cavity) with one of the possible electromagnetic mode [3]

For higher dimensions point defects can be created by locally modifying the refractive index, displacing one of the periodic patterns or changing the size. Two possibilities are shown in Fig. 8 together with the band diagram. Thus, a point defect can either push up a single mode from the band edge or pull it down. In the case where the band gap is not omnidirectional the point defect leads to a leaking of a fraction of the electromagnetic field from the point defect away into the direction in which the propagation is allowed. Is the band gap complete the electromagnetic field is concentrated at the defect.

If two point defects are introduced in a crystal with a large distance everything will remain as described above with the difference that it behaves as if the single mode is degenerated. However, when the distance is small enough it occures a second mode. The two modes represent a symmetric and a antisymmetric distribution of the electric field in analogy to the quantum mechanical situation when a particle is released in a potential well [9]. This phenomenon is called coupling of point defects.

2.3.2 Extended Defects

Extended defects can only occure in higher dimensional systems. The most studied is the 1D case which can be recieved by aligning indentical point defects. If the distances are small enough a coupling appears and leads to numerous modes appearing in the band gap. For an infinit number of defects might this result in a transmission band. The Fig. 9 shows a one dimensional defect in a two dimensional crystal where one line of rods is substituted by rods with a different reflective index. The band diagram for that can be seen on the right side of the figure.

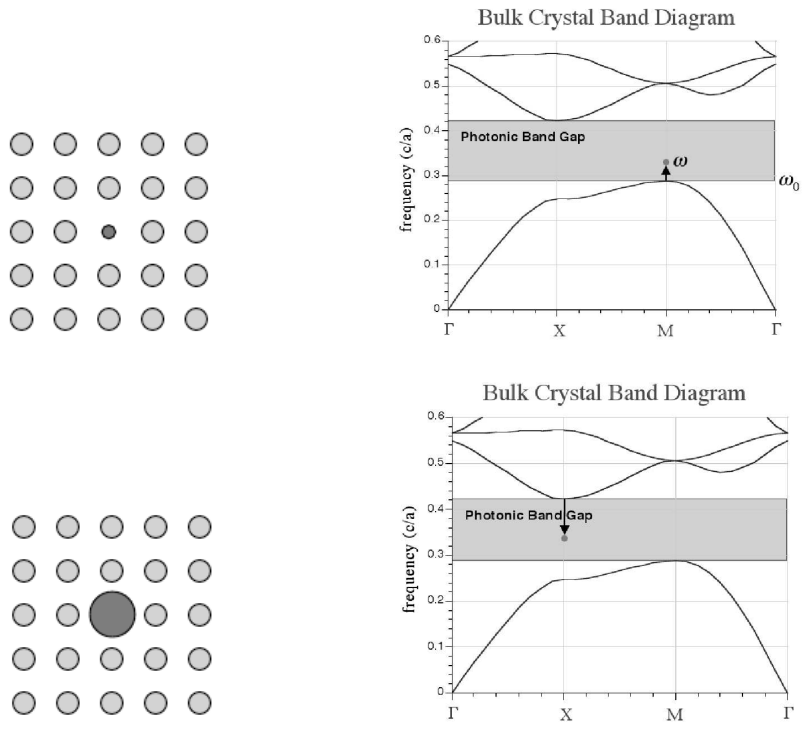

Fig. 8: *Left.* Smaller/Bigger pattern as point defect in a lattice. *Right.* Band Diagram with singel modes in the band gap [8]

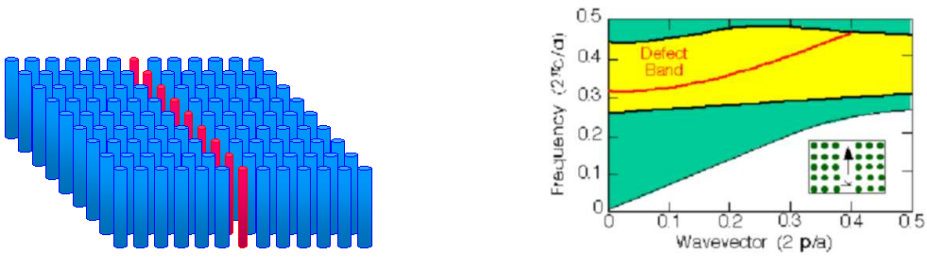

Fig. 9: *Left.* 1D defect in a 2D crystal out of rods [10]. *Right.* Band Diagram with transmission mode in the band gap for a removed row of rods [11]

2.4 Density of States

The photonic density of states (DOS) is analog to the electric density of states defined as the number of electromagnetic modes allowed per frequency unit. In the same way as the electronic DOS in a semiconductor underlies a modification from free electrons to electrons in a lattice, the density of photonic states changes when the material is structured at the scale of optical wavelengths.

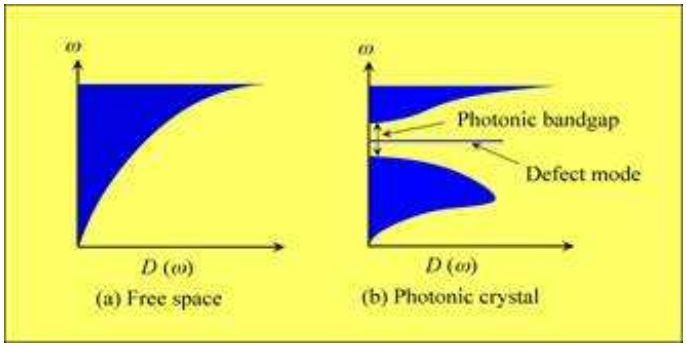

Fig. 10: Density of states in free space (*left*) and in a photonic crystal with a defect mode whithin the band gap (*right*) [12]

Generally the DOS is defined by

$$D(\omega) = \frac{\partial N(\omega)}{\partial \omega}\,, \tag{18}$$

where $N(\omega)$ is the number of eigenmodes in a volume V of eigenfrequencies less than ω. Taking into account that there are two polarizations for each vektor $\boldsymbol{k}$ the DOS in free space with the dispersion relation $\omega = ck$ is [4]

$$D(\omega) = \frac{\omega^2 V}{\pi^2 c^3}\,, \tag{19}$$

where c is the velocity of light in the material. For photonic crystals this equation is no longer valid as a consequence of a different dispersion relation $\omega(\boldsymbol{k})$. The DOS in this case is calculated by counting all allowed states with a given frequency [4] which leads to an integral over the first Brillouin zone depending on the dispersion relation. Both solutions are shown in Fig. 10.

The DOS in a photonic crystal becomes zero within the band gap i.e. there are no allowed states in this region as it is expected in a band gap. This plays an important role for the inhibition of spontaneous emission: if the photonic band gap overlaps the electronic band edge electron-hole radiative recombination will be inhibited [2]. Near the edges of the gap the DOS has maxima which also occur at every other point where the group velocity

$$v_g = \frac{d\omega}{dk} \tag{20}$$

is zero. Since the group velocity is the slope of the function $\omega(k)$, it is easy to find areas of small v_g out of the band diagram. This points are very interesting for applications like superprism, where the light propagation is extraodinary angle-sensitive [13], or gas detectors (Chap. 4.2), where the cross section for the stimulation with light plays a decisive role. As it is implied in the Fig. 10, defects cause singularities in the DOS within the photonic band gap and forming single electromagnetic modes as described in Chap. 2.3.

3 Fabrication

Most of the fabrication techniques for 2D photonic crystals, like electron beam lithography and selective etching, are adopted from the semiconductor industry. We will give a short summary about the most common materials, the fabrication process and the properties of the material. Since 2D PhCs do not possess a complete PBG it limits the set of applications, as spontaneous emission isn't suppressed in all directions and the structures show scattering losses in the third dimension. Therefore we will point out transfer possibilities to 3D PhCs, where its possible. Additionally, we present two independent techniques, the self-assembly of sub-micrometer spheres in artificial opals and holographic lithography.

3.1 Standard Fabrication

Because ordered porous dielectric materials like porous silicon or porous alumina are intrinsically 2D photonic crystals, several groups worked on ways to produce regular, ordered structures with good reproducibility. The most studied materials are porous alumina Al_2O_3 and macroporous silicon, and—more recently—porous III-V compounds. In this paragraph we refer to the summary given by R. B. Wehrspohn et al. [14].

Porous p-Type Silicon

Porous p-type silicon is formed by anodization of p-type silicon in hydrofluoric acid. Three different pore formations as a function of the dopant concentration have been observed.

For degenerately doped silicon, a special type of mesopores has been observed experimentally and explained by tunneling of holes through the space charge region. Their size is typically in the range of $5 - 50\,\mathrm{nm}$. For moderately doped silicon, micropore formation is observed. The poresize shows typical values between $2 - 5\,\mathrm{nm}$. For highly resistive silicon, macropore formation with poresizes between $0,4 - 10\,\mu\mathrm{m}$ is observed below a thin layer of micropores. In the macroporous regime, these pores can grow either in a current-limited order (low current density) or in a crystallographic order (high current density). These two regimes can be distinguished easily by the shape of the pores. If the pores have a pyramidial tip and no micropores inside of the macropores, they grew in the crystallographic regime. Typically, the crystallographic regime is used to obtain ordered arrangements of pores. In the production process, a silicon wafer with (100)-orientation is patterned by standard photolithography first. Afterwards initial seed-pores are produced by alkaline etching. The hydrofluoric etching starts selectively at these etch pitches.

Porous n-Type Silicon

Porous n-type silicon can be used as well. Since holes, which are necessary for the dissolution reaction in hydrofluoric acid, are minority carriers in n-type silicon, they have to be generated by backside illumination of the wafer. Then, they diffuse to the

etch front, where they dissolute, mainly at the pore-tips. Because of the fact, that in this technique the holes move by diffusion (and not by drift, as in the p-type case), the boundary condition of a fully depleted pore-wall is vanished and thicker walls can be optained. The process steps principally are the same as above. The arrangement of the pores can be controlled by the lithographic mask, the pore diameter by the backside illumination intensity. Hence, the pore diameter can even be modulated during the growth, which can be used for the production of 3D photonic crystals.

Fig. 11: *Left.* Ordered porus n-type silicon ($a = 500\,\mathrm{nm}$). *Right.* Selfordered mesoporus silicium ($d = 500\,\mathrm{nm}$) self-organised in a hexagonal array [14].

Porous Alumina

Aluminium is electrochemically oxidized to alumina. An absorbing relationship between the anodization voltage U and the interpore distance a was found: $a = d + 2\alpha U$, where d is the pore-diameter and $\alpha \approx 1.2\,\mathrm{nm/V}$. After a long anodization time, hexagonal close-packed patterns of pores can be obtained by self-organisation. The size of the ordered pore domains increases with time and can reach micron size.

Since electron beam lithography is a planar technique, it is not straightforward to transfer this method to the fabrication of 3D PhCs. A possible way to overcome this problem is the production of layer-by-layer-samples. The size of these crystals is limited by the complexity of the production process, e.g. high mechanical precision, to a few periods.

3.2 New Techniques of Fabrication

3.2.1 Holographic Lithography

Light fields from multiple beam interference can be used to fabricate PhCs since the light distribution is spatially (quasi-)periodic with a period of the order of half the wavelenght [15]. The interference pattern can be recorded as a volume hologram and converted into correspondingly structured matter distribution. Photoresists are used as a recording medium.

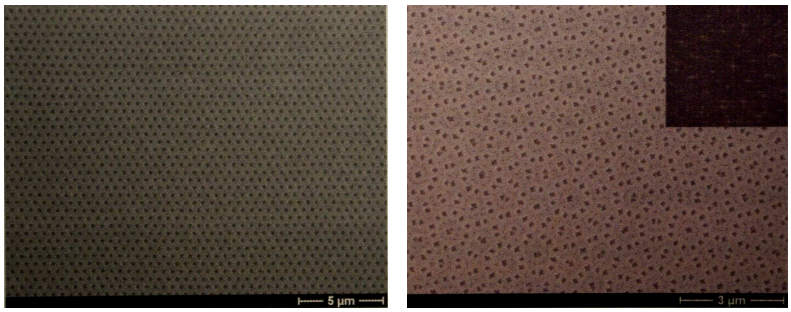

Fig. 12: *Left.* Ordered porus alumina with $a = 500\,\text{nm}$ obtained by imprint lithography. *Right.* By repeated imprint under an angle of 2.2 degrees, a 12-fold symetry can be obtained [14].

3.2.2 Crystallization of Artificial Opals

This technique makes use of the self-assembly of preformed colloids or beads into a face centered cubic (fcc) packing [16] as shown in Fig. 13. This material has basically the same structure as natural occurring opals, however, the latter are locally heterogenous, composed of various crystallites and differing in the size of the beads. The diameter of these beads fixes the optical properties of the resulting photonic crystal. Beads of a diameter in the range of several hundred nanometers, which corresponds to the wavelength of visible light, have been produced. The most common material is SiO_2, whereas more recently polymer beads came up.

A precondition and the main challenge in the preparation of artificial opals is the preparation of monodisperse beads or colloids. The use of different inorganic materials offers a very broad variability of optical properties due to their variability of size, but it is not yet possible for most materials, except SiO_2, to achieve monodiserpsity at a satisfactory level. Polymer or organic colloids offer the advantage that monodisperse particles can be obtained more easily and that they can be functionalized easily e.g. with fluorescent dyes.

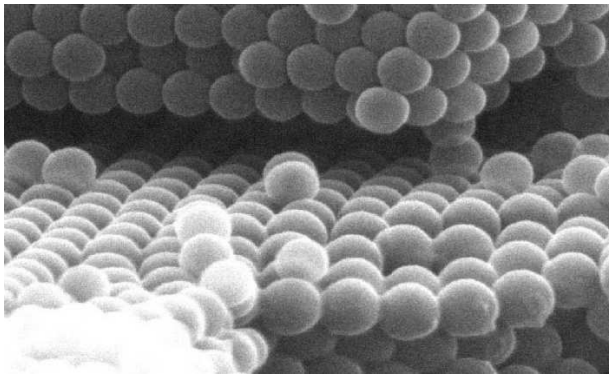

Fig. 13: Natural occuring fcc opal structure [17]

4 Application

Our theoretical introduction into the properties of photonic crystals (Chap. 2) shows that they can be seen as an “optical semiconductors“ in many cases. Hence, the hope raises that their special properties can be used in many applications and in what follows, we want to introduce tree of them: optical fibres, gas sensors and lasers.

4.1 Fibres

The most popular application of photonic crystals surely are photonic crystal fibres (PCF) which are allready since several years at the stage of commercial production and have a huge field of usage.

4.1.1 Configuration

The standard optical fibre consists of a fibre core surrounded by a lower index cladding, thus light is confined by total reflection. A new type of optical fibres makes use of photonic crystals. One can distinguish two main versions which are shown in Fig. 14: the Holey fibre (a) and the PBG-fibre (b). The guiding mechanism is provided either by means of modified total internal reflection in Holey fibres or a photonic band gap effect in PBG fibres. Although the same material is used for core and cladding for the Holey fibre, the incorporation of air holes in the cladding area results in an effective lowering of the refractive index. Holey fibres with large air filling fraction resulting in a high effective index-difference are called High-Delta or Cobweb fibres. Field confinement in an air-core fibre, based on the band gap effect, requires a periodic arrangement of air holes on a wavelength scale with a sufficiently high air filling fraction in the cladding [18].

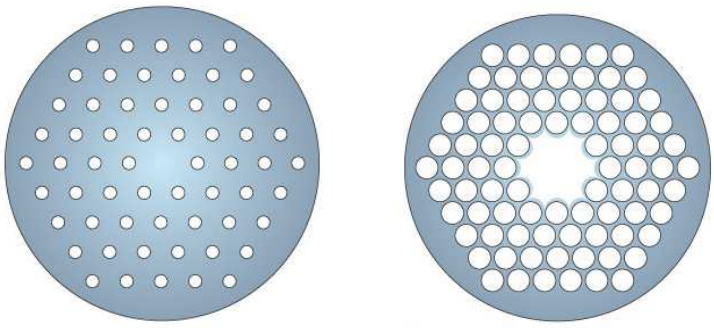

(a) Holey Fibre (b) PBG Fibre

Fig. 14: Main versions of fibres out of photonic crystals [19]

4.1.2 Preparation

The usual way to prepare optical fibres with a microstructured cross section is to stack capillaries and solid rods to form a compound structure, which resembles the desired fibre cross section. The final diameters are realized during the following draw down, where the capillaries have to be combined with each other, but without closing the holes completely. A new approach [20] is extrusion, in which molten glass is forced through a die containing a suitably designed pattern of holes. Extrusion allows fibre to be drawn directly from bulk glass, and almost any structure from crystalline to amorphous can be produced. Functional defects could be precisely introduced during the stacking process, allowing fabrication of a wide range of different sort of photonic crystal fibres.

4.1.3 Application

The first working photonic crystal fibre was produced in 1996 [21], which consisted of an array of 300 nm-airholes, spaced 2.3 μm apart, with a solid core in the middle. The most remarkable property of this fibre was that the fibre did not become multimode in the experiments, no matter how short the wavelength of the light was.

This interesting "endlessly single-mode" behavior can be understood by viewing the array of holes as a modal filter or "sieve". The fundamental mode fits into the core, filling the diameter with one single lobe. However, for higher order modes, the dimensions of the lobes are getting smaller and they can slip between the gaps. Correct choice of geometry thus guarantees that only the fundamental mode is guided through the fibre. Every other mode leaks out after a short distance which is pointed up in Fig. 15.

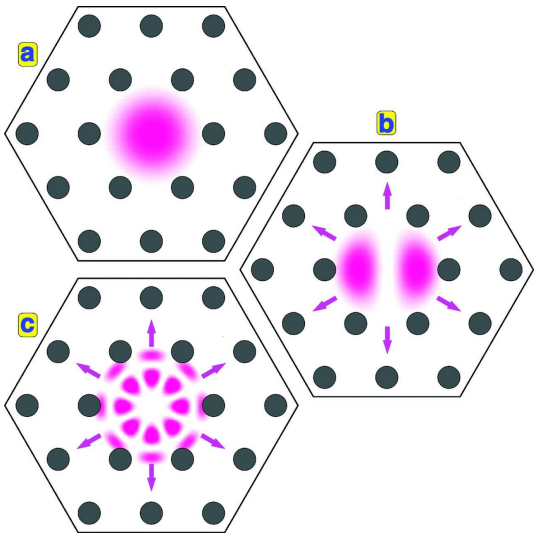

Fig. 15: "Endless single-mode": Only one mode is localised in the core and its energy is conserved (a), all other modes are leaking out (b), (c) [20]

Another advantage is, that traditional optical fibres suffer additional loss, if they are bent more than a critical radius. This radius depends on wave-length, geometry and

core/cladding-refractive index step. Because of the different guidance principle photonic crystal fibres escape theses effects.

Beyond the features offered by conventional optical fibres, photonic crystal fibres are finding an increasing number of further applications. We'll sample a few of them referring to [20]:

High harmonic generation. Another field where hollow-core fibre is likely to play a big role is that of high harmonic generation. When gases such as argon are subjected to ultrashort high-energy in the range of fs and pulses in the range of mJ, the extremely high, short duration electric field momentarily ionizes the atoms, and very high harmonics of the laser frequency are generated during the recombination process. Ultraviolet and even x-ray radiation can be produced in this way. It is of interest, that hollow-core PCF could bring this process within the reach of compact diode-pumped laser systems, potentially leading to table-top x-ray sources for medicine, lithography, and x-ray diagnostics.

Atom and particle guidance. First shown in the 1970s, small dielectric particles can be trapped and levitated in a laser beam using the dipole forces exerted by light. Nowadays, atoms, molecules, particles and biologic cells can be trapped and manipulated with very high precision. A related area is that of atom and particle transport along hollow capillaries, where the optical dipole forces of a laser beam prevent adhesion to the glass surfaces and provide the acceleration needed to overcome viscosity.

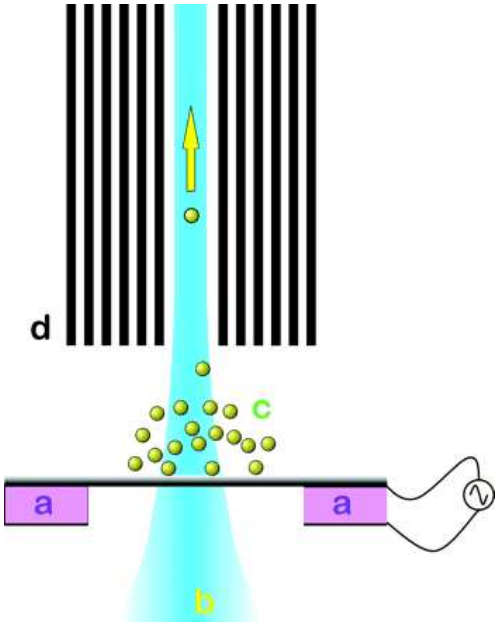

Fig. 16: Schematic sketch of atomtransport via PCFs: Van der Waals bonds between plate and atoms/molecules (c) are overcome by piezoelectrically generated vibrations (a) levitated by the beem (b) and conducted into the PCF (d) [20]

Here, the absence of a single guided mode in the capillary limits the effectiveness of the technique. Large ($\sim 200\,\mu$m) and hence multi-mode bore capillaries must be used to avoid leakage, which means that adequate trapping forces can be obtained only at high laser powers. Hollow-core PCF provides a good solution to this problem, as shown in recent experiments, where only 80 mW of 514 nm argon laser light was sufficient to levitate and guide $5\,\mu$m polystyrene spheres along a 15 cm length of PCF with a hollow-core diameter of $20\,\mu$m. This technique is about to be extended to the guidance of atoms and molecules which is illustrated in Fig. 16.

Ultrahigh nonlinearities. PCFs with extremely small solid glass cores and very high air-filling fractions not only display unusual chromatic dispersion but also yield very high optical intensities per unit power. Thus one of the most successful applications of PCF is to nonlinear optics, where high effective nonlinearities, together with excellent control of chromatic dispersion, are essential for efficient devices.

4.2 Gas Sensors

Gas sensors are widely used in medical and environmental applications. Optical gas sensors make use of the characteristic absorption lines in the mid infrared wavelength region of $3-20\,\mu$m. Traditional sensors are based on spectroscopicy techniques but with the big drawback of high production costs. The advantage of an optical gas sensor based on photonic crystals could be the possibility of miniaturization, integration and thus cost reduction. For this application, macroporous silicon is the material of choice, as structures for optical detection in the mid-infrared region can be fabricated with good reproducibility.

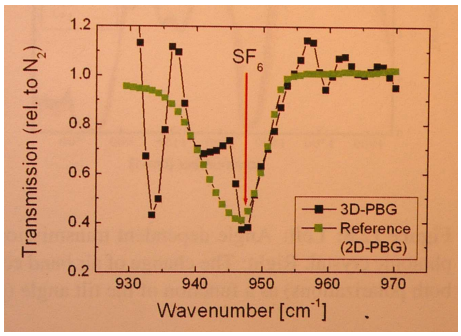

Fig. 17: Transmission of the 3D PhC filled with SF_6 normalised to that filled with N_2 (black) and compared to 2D PhC with the same porosity (green) [22]

An optical sensor consists of three basic parts: the radiaton source, the absorption section and the detector. For a traditional gas sensor, the length of the absorption section is in the range of $10-50$ cm to achieve a good signal-to-noise-ratio. This results in a large volume with several practical limitations. By using photonic crystals, these typical length can be scaled down into the micrometer range [22].

We will explain a short scheme of the principle: At the band edges of a photonic crystal, we find very strong spectral dependence of the group velocity. Near the band edges the bands are extremely flat. This gives rise to a very small group velocity, which is defined as the slope of the dispersion relation. The group velocity goes to 0 as the frequency approaches the band edge. The small group velocity extends the time the photons need to travel through the structure. Thus, the propability of interactions between the light field and the atoms is increased. On the other hand, the low group velocity enhances the effective refractive index, which increases the reflection at the interface PhC/surrounding material. Both effects lead to a higher absorption of light.

Wehrspohn et al. [14] tested this thought on a 3D macroporous silicon sample. They adjusted the modulation period by electrochemical etching, so that the upper band edge coincidences with the absorption line of SF6 at 948 cm^1). The result is shown in Fig. 17. The spectrum obtained is rather noisy, which results from the low coupling efficiency due to the high effective refractive index. This can be improved by using an adiabatic taper. The easiest approach would be a device, where the lattice constant is increased towards the interfaces.

4.3 Lasers

Lasers like in Fig. 18, which makes use of photonic crystals as tunable mirrors have been used for a while. One of the drawbacks of the combination of a ridge waveguide laser with a PhC waveguide is their large modal mismatch. Although taper structures can be used, they add unnecessary complexity to the devices. The coupling issue can be avoided by using "all PhC lasers", where the resonator is formed by a PhC waveguide [23]. We'll give a short presentation of these devices.

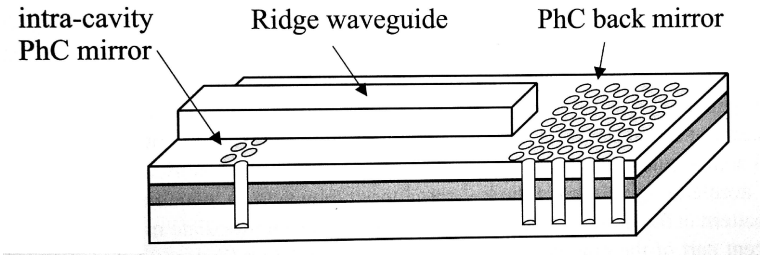

Fig. 18: Ridge waveguide laser setup using PhCs as high reflective mirrors [23]

A simple PhC waveguide would be sufficient but this laser would give a multi-mode spectrum. In order to obtain single mode operation, one has to add a wavelength selective element into the resonator. Kamp et al. [23] found, that one can use a design with a chain of coupled hexagonal resonators as shown in Fig. 19(a). The coupling of the cavities leads to a formation of minibands within the photonic bandgap. Due to the wide spacing of the minibands (approximately 100 nm) only one miniband will be spectral region with substantial gain, so the lasing operation will be restricted on this particular miniband. Obtained spectra can be seen in Fig. 19(b).

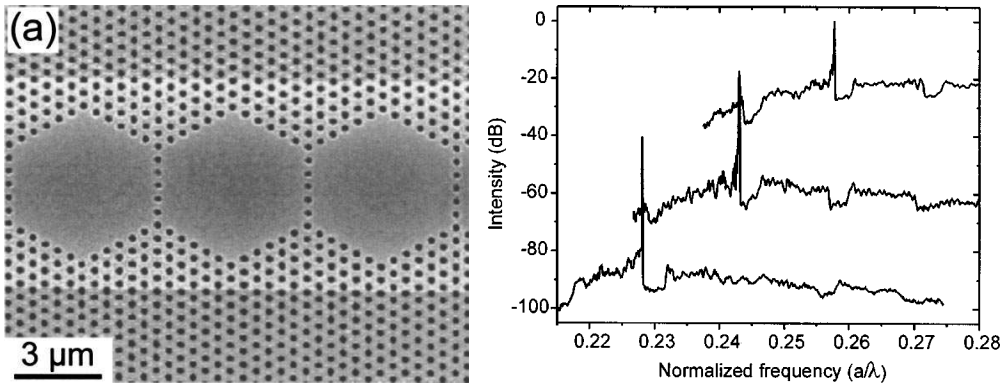

(a) SEM micrograph (b) Laser spectrum

Fig. 19: CROW patterned PhC with corresponding laser spectra for different lattice constants $a = 350, 375, 400\,\text{nm}$. In the spontaneous emission background one can see several "stop-bands" separating the miniband regions [24]

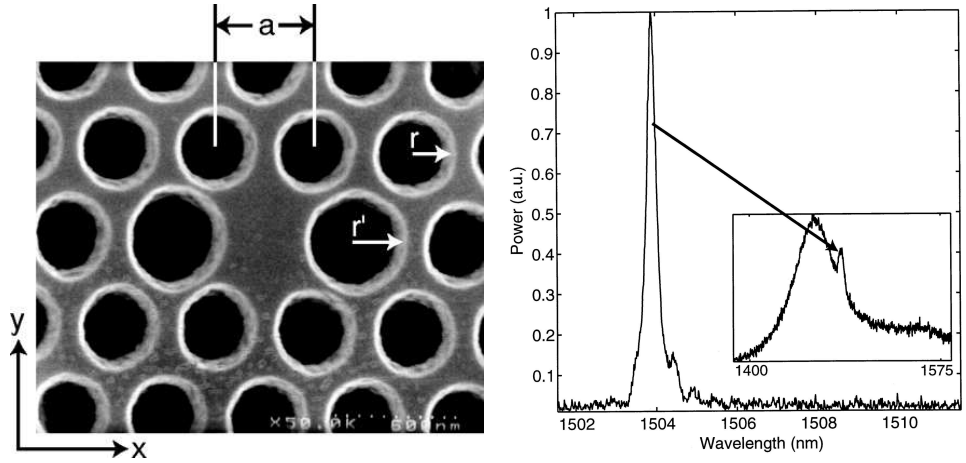

(a) (b)

Fig. 20: Microcavity laser together with the laser spectrum [25]. (a) shows the top view of the hexagonal 2D array of air holes with a missing central hole which forms the cavity. The result of the two enlarged holes is a single mode cavity in which only the y-dipole mode is well localised. (b) shows the spectrum just above the threshold. The inset shows the spontaneous emission spectrum

Another possible application of PhCs in the laser field are microcavity lasers. We wil present an example, where the cavity is formed by a single defect in a 2D photonic crystal [25]. The ability to fabricate compact microcavity light sources is essential for the construction of future optical curcuits. One advantages of using PhCs is the broad flexibility in geometry, which leads to fine-tuning of the emission spectrum. Additionally, the high spontaneous emission coupling factor β and the compact size make it interesting, to use microcavity lasers as a low-noise and low-threshold light source.

The light is confined into the cavity by two different mechanisms. First, a $\lambda/2$-slab of high refractive index is used to limit vertical freedom of the photons by way of total internal reflection. Second, the light is localized in the plane by a 2D photonic crystal. By removing one (or more) of the holes in the photonic crystal pattern, a defect-cavity is created such as the Fig. 20(a) it shows. The resonant mode is highly localized into this defect region and can only escape by either tunneling through the photonic crystal or by striking the slab at a sufficiently high angle to leak out in vertical direction. A spectrum of the laser is shown in Fig. 20(b). The spontaneous emission below threshold results from emissions from the surrounding, unprocessed area excited by the pump beam. The linewidth is below 0.2 nm which represent the resolution limited. Until now, it is not possible to use microcavity lasers at room temperature and continuous operating. The reasons are that the threshold pump power is still too high due to the low quality factors reached by standard fabrication, and that the heat regulation techniques aren't sufficient yet.

5 Conclusion

More than 15 years after the first realisation of a full photonic band gap, photonic crystals still remain a prosperous part of research and more and more of economic application.

From the theoretically point of view, PhCs provide the opportunity to combine the existing knowledge of different fields especially solid state physics and optics together with new mathematical modelling studies and nonlinear dynamics due to the fact that the mathematical structure for PhCs is more complicated for example in the three-dimensional case or when combining it with active materials like emitters.

But photonic crystals are on the way from an exclusively scientific topic to the origin of economic applications which are using the unique properties of this materials for inventing new products or advancing existing devices. Often it is not necessary to have a full band gap for applications. The effect of the very low group velocity at the band edges, for example, leads to a variety of capabilities especially in processes of small cross sections like gas detectors. On the other hand photonic crystals as "optical semiconductors" raise the hope to create optical devices and photonic circuits as the future of classical semicoductor microtechnology. Fibres out of 2D photonic crystals, which are already commercial produced, surely form a cornerstone in this field with the possibility of lossless transport of light even through sharp bands. This offers together with the research in 3D PhCs new options for the complete controlling of light, constructions of optical devices in the micrometerscale and finally applications like optical computers. Many problems like in the accurate production of higher dimensional photonic crystals must sill be solved to reach this goal but with the continuous development in nano- and microtechnology this comes into reach within the next decades.

References

[1] E. M. Purcell. Resonance absorption by nuclear magnetic moments in a solid. *Phys. Rev. 69:681*, 1946.

[2] E. Yablonovitch. Inhibited spontaneous emission in solid-state physics and electronics. *Phys. Rev. Lett., 58:2059*, 1987.

[3] Jean-Michael Lourtioz. *Photonic Crystals - Towards Nanoscale Photonic Devices*. Springer-Verlag Berlin Heidelberg, 2005.

[4] K. Sakoda. *Optical Properties of Photonic Crystals*. Springer-Verlag Berlin Heidelberg, 2001.

[5] S. G. Johnson and J.D. Joannopoulos. Introduction to photonic crystals: Bloch's theorem, band diagrams, and gaps. 2003.

[6] Ch. Kittel. *Introduction to Solid State Physics*. John Wiley and Sons, Inc., 2004.

[7] E. Yablonovitch, T.J. Gmitter, and K.M. Leung. Photonic band structure: The face-centred-cubic case employing nonspherical atoms. *Phys. Rev. Lett. 67:2295*, 1991.

[8] `http://ab-initio.mit.edu/photons/tutorial/L2-defects.pdf`.

[9] C. Cohen-Tannoudji, B. Diu, and F. Laloe. *Quantum Mechanics*. Wiley-Interscience, 2006.

[10] `http://cumsl.msl.columbia.edu/optics/nicolae/NonlinPhotCryst.html`.

[11] `http://ab-initio.mit.edu/photons/bends.html`.

[12] `http://www.nims.go.jp/nanophoto/PC.htm`.

[13] H. Kosaka and et al. Superprism phenomena in photonic crysals. *Phys. Rev. B 58:R10096*, 1998.

[14] R. Wehrspohn and et al. Electrochemically-prepared 2d and 3d photonic crystals. *Photonic crystals - Advances in Design, fabrication and characterization; Wiley-VCH*, 2004.

[15] A. Blanco and et al. Three-dimensional lithography of photonic crystals. *Photonic crystals - Advances in Design, fabrication and characterization; Wiley-VCH*, 2004.

[16] M. Egen and et al. Preparation of 3d photonic crystals from opals. *Photonic crystals - Advances in Design, fabrication and characterization; Wiley-VCH*, 2004.

[17] `http://www.tyndall.ie/projects/phat/summary.html`.

[18] J. Kirchhof and et al. Photonic crystal fibers. *Photonic crystals - Advances in Design, fabrication and characterization; Wiley-VCH*, 2004.

[19] J. Knight. Photonic crystal fibers. *Nature 424*, 2003.

[20] P. Russel. Photonic crystal fibers. *Science 299*, 2003.

[21] J. C. Knight, T. A. Birks, P. St. J. Russell, and D. M. Atkin. All-silica single-mode fiber with photonic crystal cladding. *Opt. Lett. 21:1547-1549*, 1996.

[22] S. Schweizer and et al. Application of photonic crystals for gas detection and sensing. *Photonic crystals - Advances in Design, fabrication and characterization; Wiley-VCH*, 2004.

[23] M. Kamp and et al. Photonic crystal based active optoelectronic devices. *Photonic crystals - Advances in Design, fabrication and characterization; Wiley-VCH*, 2004.

[24] T.Happ and et al. Two dimensional photonic crystal coupled-defect laser diode. *Appl. Phys. Lett. 82*, 2003.

[25] O. Painter, R.K. Lee, and A. Scherer. Two dimensional photonic band-gap defect mode laser. *Science 284*, 1999.